

Interstellar dust

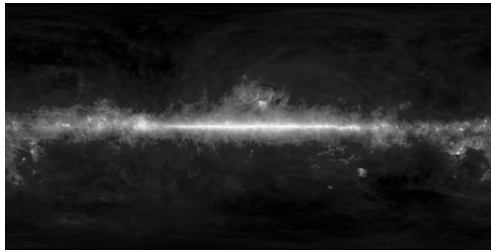
All astronomers need to know about dust

Extinction affects our measurements of distant objects, and has to be corrected for in any quantitative analysis

Foreground dust (and molecular) emission overlies the cosmic microwave background emission and has to be modelled and subtracted to reveal the true CMB distribution.

Dust accounts for ~50% of the heavy elements, and the building blocks of life

Even though dust is less than 1% of the baryonic mass of the Galaxy, it emits ~40% of the total luminosity



Useful References include:

Interstellar Dust Grains, B.T. Draine, Ann Rev Astr Ap 2003 vol 41, p241-289
Dust in the Galactic Environment, D.C.B Whittet 2nd ed 2002, IoP publishing

Cosmic Dust

Evidence from:

Extinction (and polarization) of starlight

Infrared emission from particles with $10 < T < 1000\text{K}$

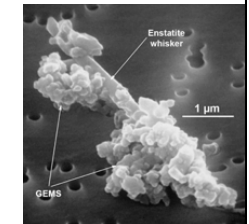
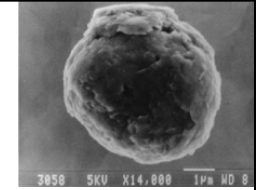
Spectroscopic identification of absorption and emission bands

Depletions of gas-phase refractory elements

Reflection nebulae

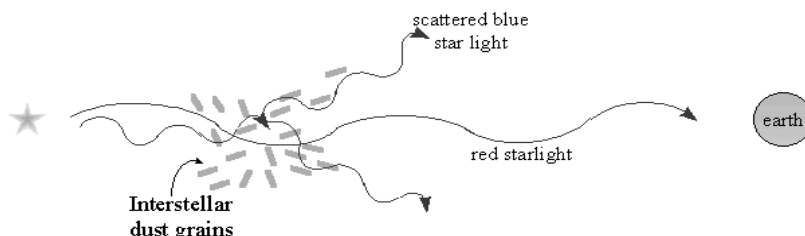
In-situ measurements of meteorites and interplanetary dust particles

But detailed physical and chemical properties remain uncertain



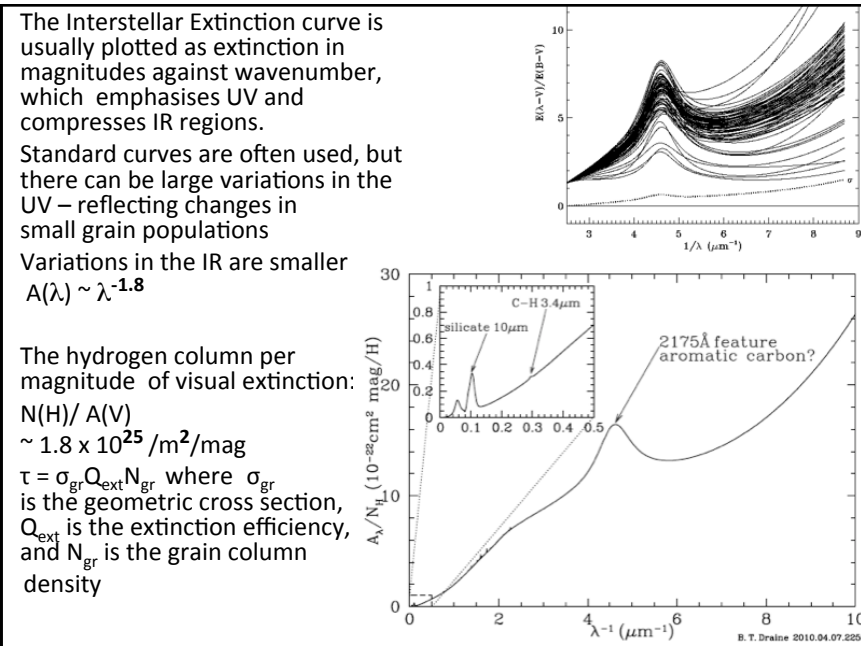
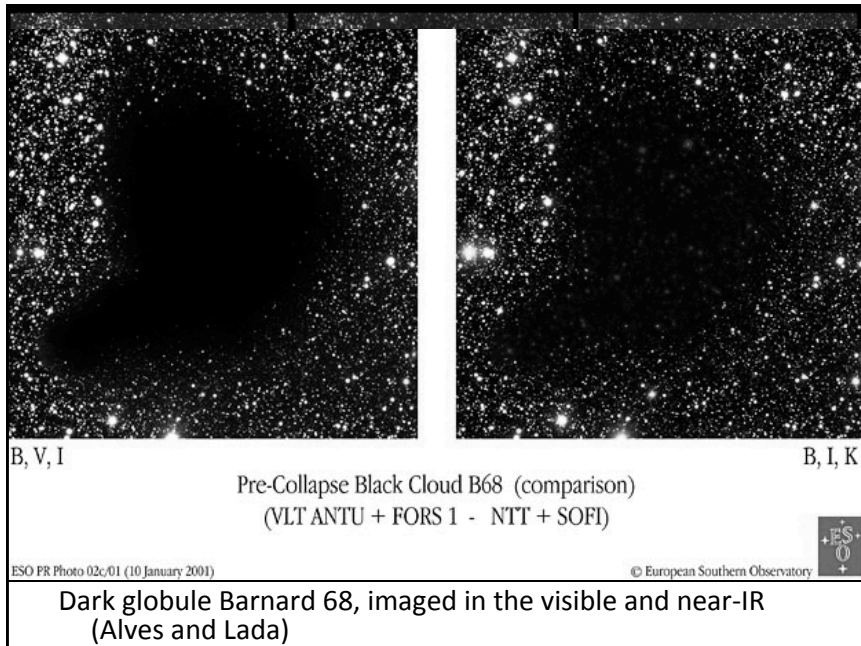
Interstellar Reddening

- Distant stars appear redder than nearby examples
- Attributed to scattering by small particles with size $\sim \lambda$ - cosmic dust
- Extinction = scattering + absorption
Structure in the extinction curve provides information on the dust particles
- Scattering efficiency falls with increasing wavelength and becomes unimportant in the infrared where absorption dominates



The Interstellar Extinction Curve

- Generally it is not possible to look at one object to cover the whole spectrum - need to patch together observations from UV to IR.
- Extinction comprises of scattering and absorption terms:
 $Q_{\text{ext}} = Q_{\text{scat}} + Q_{\text{abs}}$ where the grain albedo $w = Q_{\text{scat}}/Q_{\text{ext}}$
- When $\lambda \gg a$, Rayleigh scattering holds, which falls as $Q_{\text{scat}} = \lambda^{-4}$. The absorption term $Q_{\text{abs}} \approx \lambda^{-1}$, so scattering becomes unimportant at long wavelengths (in the mid and far-IR) and absorption dominates.
- Dust grains come in a range of sizes (and probably shapes), with the smallest grains having the most effect at short wavelengths. Need grains with characteristic size $2\pi a \sim \lambda$ for efficient scattering: dust responsible for visible extinction has a $\sim 0.1\mu\text{m}$
- Different lines of sight reveal differences in detail attributed to changing dust grain sizes and/or mixture of species, but gross properties are maintained



Dust towards the Galactic Centre

Infrared spectrum of the Galactic Centre, Sgr A, which is viewed through large columns of dusty ISM material. IR absorption Bands at 10 and 20 μm are attributed to absorption by silicate dust and at 3.4 μm by hydrocarbons. The extinction in the visible is $A(\text{v}) \sim 30\text{mag}$ rendering the GC invisible, so it can only be probed at long wavelengths. In this plot, the wavelength dependence of extinction is estimated from the measured fluxes of Hydrogen recombination lines, compared to those calculated from recombination theory.

THE ASTROPHYSICAL JOURNAL, 737:73 (21pp), 2011 August 20

FRITZ ET AL.

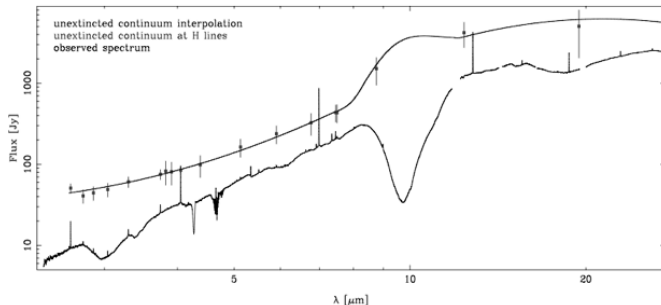


Figure 10. Measured and unextincted MIR continuum toward the GC. The black line is the observed ISO-SWS spectrum. We unextinct the continuum around the hydrogen lines by the hydrogen line extinctions there (red boxes). We interpolate these points to obtain the unextincted continuum (blue line).

Dust in the Interstellar Medium

Circumstellar Dust is injected into the ISM from cool stars (RGB, AGB) and novae, supernovae etc.

Dust injected from stars in the Milky Way :

It is processed in the various phases of the ISM, including growth via coagulation, condensation of icy materials and erosion through sputtering and shocks.

The balance between grain injection and destruction is not understood but calculated destruction timescales are faster than injection rates, implying that dust is replenished in the ISM

| Type | Total Number | Amount (M_{\odot}/yr) |
|---------------|--------------|----------------------------------|
| Mira | 9000000 | 2 |
| OH/IR | 60000 | 2 |
| Carbon | 40000 | 0.6 |
| Supernovae | 1/50yr | 0.2 |
| M Supergiants | 5000 | 0.2 |
| OB Stars | 50000 | 0.1 |
| WR Stars | 3000 | 0.05 |
| PN | 4000 | 0.2 |
| Novae | 50/yr | 0.0001 |

Dust grain abundances from depletions

Table 23.1 Inferred Elemental Composition of Dust toward ζOph

| <i>X</i> | $(N_X/N_H)_\odot^a$ (ppm) | $N_{X,gas}/N_H^b$ (ppm) | $N_{X,dust}/N_H$ (ppm) | $10^3 M_{X,dust}/M_H$ (ppm) |
|---|------------------------------|---|----------------------------------|--|
| C | 295 ± 36 | 135 ± 33 ^{d,e} | 160 ± 49 | 1.92 ± 0.59 ^e 210 ± 41 2.52 ± 0.49 ^f |
| N | 74.1 ± 9.0 | 78 ± 13 ^g | -14 ± 16 | 0 |
| O | 537 ± 62 | 295 ± 36 ^d [383] ^c | 242 ± 72 154 ± 8 ^c | 3.87 ± 1.15 2.46 ± 0.13 ^c |
| Mg | 43.7 ± 4.2 | 4.9 ± 0.5 ^g | 39 ± 4 | 0.94 ± 0.10 |
| Al | 2.8 ± 0.2 | 0.005 ± 0.001 ^h | 2.8 ± 0.2 | 0.08 ± 0.01 |
| Si | 35.5 ± 3.0 | 1.7 ± 0.5 ⁱ | 34 ± 3 | 0.95 ± 0.08 |
| S | 14.5 ± 1.0 | 28 ± 16 ^j | -14 ± 16 | 0 |
| Ca | 2.3 ± 0.2 | 0.0004 ± 0.0001 ^k | 2.2 ± 0.2 | 0.09 ± 0.008 |
| Fe | 34.7 ± 3.3 | 0.13 ± 0.01 ^g | 35 ± 3 | 1.96 ± 0.17 |
| Ni | 1.7 ± 0.2 | 0.0030 ± 0.0002 ^j | 1.7 ± 0.2 | 0.10 ± 0.01 |
| Total if $f(\text{C II}]2325) = 4.78 \times 10^{-8}$ (see text) | | | | 9.9 ± 1.3 ^e |
| Total if $f(\text{C II}]2325) = 1.0 \times 10^{-7}$ (see text) | | | | 10.5 ± 1.3 ^f |
| Total if $f(\text{C II}]2325) = 1.0 \times 10^{-7}$, $N_{O,dust}/N_H = 154$ ppm (see text) | | | | 9.1 ± 0.6 ^e |

^a Asplund et al. (2009).
^b Assuming $N(\text{H}) + 2N(\text{H}_2) = 10^{21.13 \pm 0.03} \text{ cm}^{-2}$.
^c Assuming $N_{O,dust}/N_H = 154$ ppm.
^d Cardelli et al. (1993).
^e If $f(\text{C II}]2325 \text{ \AA}) = 4.78 \times 10^{-8}$ (Morton 2003).
^f If $f(\text{C II}]2325 \text{ \AA}) = 1.00 \times 10^{-7}$ (see text).
^g Savage et al. (1992).
^h Morton (1975).
ⁱ Cardelli et al. (1994).
^j Federman et al. (1993).
^k Crinklaw et al. (1994).

Solar, interstellar gas phase, and inferred abundances condensed into dust along the line of sight towards ζ Ophiuchi, from B Draine 2011

TABLE 1
SOLAR AND STELLAR ABUNDANCES FOR THE DUST-FORMING ELEMENTS C, O, Mg, Si, AND Fe (RELATIVE TO 10^6 HYDROGEN ATOMS)

| Object | C | O | Mg | Si | Fe | References |
|------------|-----|-----|------|------|------|------------|
| Sun | 370 | 676 | 34 | 32 | 34 | 1 |
| | 417 | 692 | 39.9 | 37.6 | 38.8 | 2 |
| | 363 | 853 | 38.5 | 35.8 | 32.3 | 3 |
| | 331 | 676 | 38 | 35.5 | 31.6 | 4 |
| | 391 | 545 | 34.5 | 34.4 | 28.1 | 5 |
| | 245 | 490 | ... | ... | ... | 6 |
| | ... | 457 | ... | ... | ... | 7 |
| | 245 | 457 | 33.9 | 32.3 | 28.2 | 8 |
| F, G stars | 358 | 445 | 42.7 | 39.9 | 27.9 | 9 |
| B stars | 190 | 350 | 23 | 18.8 | 28.5 | 9 |

REFERENCES.—(1) Cameron 1973; (2) Cameron 1982; (3) Anders & Grevesse 1989; (4) Grevesse & Sauval 1998; (5) Holweger 2001; (6) Allende Prieto et al. 2002; (7) Asplund et al. 2004; (8) Asplund et al. 2005; (9) Sofia & Meyer 2001.

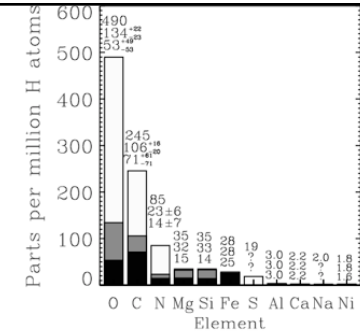


Fig. 1.5. Depictions of elements having solar abundance greater than 10^6 times that of H (excluding H and the noble gases He and Ar), with the horizontal positions arranged according to the ranks in total abundances shown by the heights of the bars. The interior of each bar is broken down by the element's fraction in gaseous form (upper, clear portion) and solid form $(X/H)_{dust}$ evaluated from Eqs. [3] and [6] according to whether $F_c = 1.0$ (gray plus black lower portions) or $F_c = 0.0$ (only the black portion). Numbers over each bar state the values (and errors, if more than 3 ppm) corresponding to the tops of the black, gray and clear zones.

Abundance constraints for major dust constituents

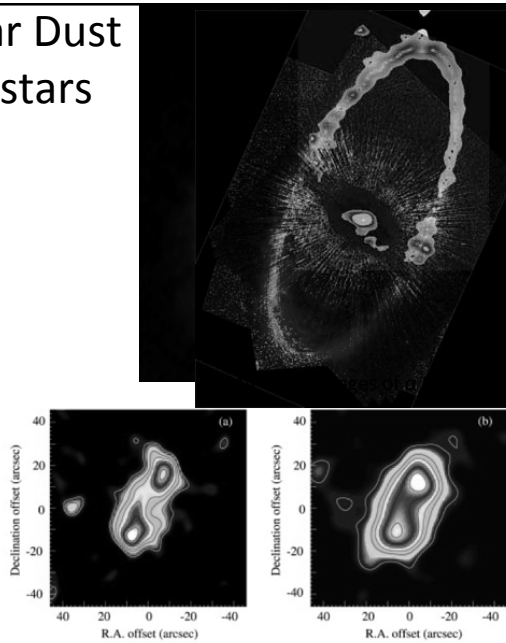
Left: Reference interstellar medium abundances obtained from 3 sources : the sun, local F & G stars and B stars (from Li 2004). Depletions are measured with respect to these.

Right: The fraction of abundant elements condensed in grains estimated by Jenkins, where the light and dark solid regions reflect the more robust and more fragile grain components.

Circumstellar Dust heated by stars

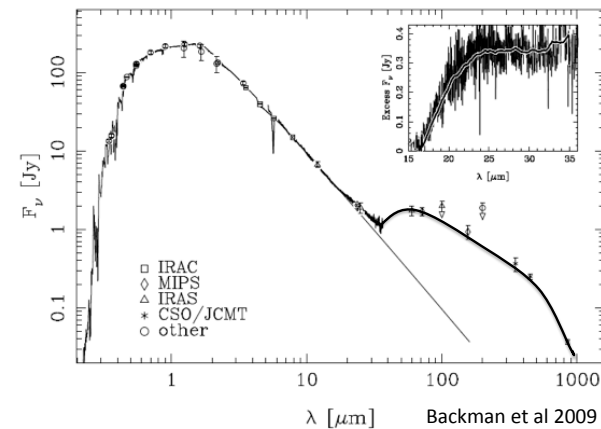
Starlight is absorbed by dust in circum-stellar environments. The dust is heated and emits in the IR.

e.g. Fomalhaut (αPsA), a young nearby (7.7pc) A star with a remnant 'debris' disk left over from its formation. Discovered at sub-mm wavelengths. Sub-mm ring $r \sim 200\text{AU}$, $T < 50\text{K}$. $M \sim 1.5 M(\text{Moon})$ with warmer inner dust emission.



JCMT/Scuba map
Holland et al 2003

Eps Eridani SED



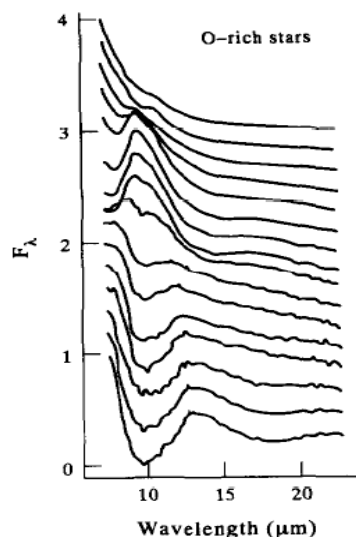
Bulk of the dusty disk material is cold, with weak emission at $\sim 15\mu\text{m}$ ($\sim 200\text{K}$). Central cavity with surrounding dusty disk. Outer material, large icy grains.

Circumstellar Dust

Dust condenses around cool stars, absorbing starlight and emitting in the IR. Dust forms in dense inner regions when $T < T(\text{condensation})$

As the rate of mass loss increases, the dusty envelopes become denser and more extensive, and in the most extreme cases, some stars can be completely cocooned within their dusty envelopes so that they are only detectable in the infrared.

The balance between C and O is a major influence on astrochemistry. Where O is more abundant than carbon, O-rich dust condenses forming Mg, Fe and Si compounds with oxygen – silicate grains. They are identified through strong, broad emission peaks at $10\mu\text{m}$ and $20\mu\text{m}$. However, as the emission becomes optically thick, these bands appear in absorption



Dust Composition

Depletion studies indicate that C, O, Mg Si, Fe must be the major constituents of cosmic dust.

Extinction indicates that Dust mass is $\sim 1\%$ of the gas mass.

Observations of cool star circumstellar envelopes, planetary nebulae etc show that the dust formed is a strong function of C/O ratio.

CO is a very stable molecule and it mops up the available C or O, with the residual amounts of the more abundant element available for other species

Where $C/O < 1$, we see silicate grains – amorphous structures, with some evidence of crystalline grains. SiO is seen in the gas phase.

$C/O > 1$ gives rise to carbon-rich grains - amorphous carbon (soot), Silicon Carbide and aromatic hydrocarbons

Polarization measurements demonstrate that silicate grains are non-spherical and can be aligned to magnetic fields

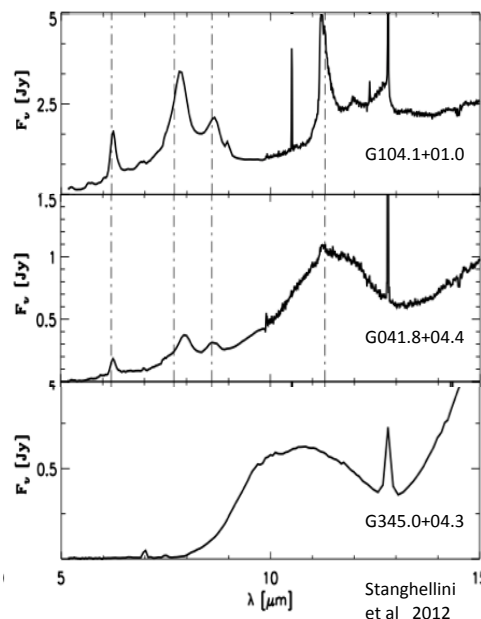
Dust signatures in Planetary Nebulae

Ionized gas in PN provides estimates of gas-phase element abundances, which are compared with the infrared spectral signatures from dust grains.

Mid-IR spectra of PN are categorized by their main emission bands as objects dominated by emission from :

- Polycyclic Aromatic Hydrocarbons PAHs (top) with a series of bands attributed to C-H and C-C bending and stretching modes
- Silicon Carbide grains (middle), a broad emission band, peaking at $11.2\mu\text{m}$.
- Silicate grains (bottom) with broad emission peaks at 9.7 and $18\mu\text{m}$.

There is good agreement between the presence of these dust components and decreasing gas phase C/O ratios



Dust dependence on C:O ratio

The PAH band emission increases with increasing C:O ratio. The most Carbon-rich objects produce more carbon-rich grain species.

The fractions of C-rich PN depend upon the metallicity and mass of the pre-cursor stars, and so we expect the type and amount of dust injected to vary in different environments.

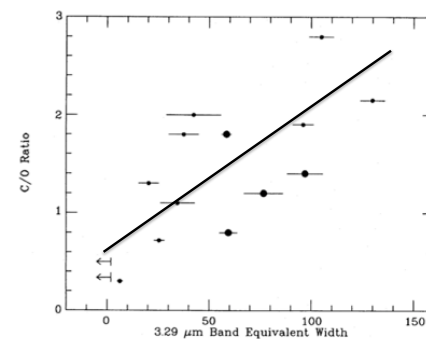


Figure 3. Carbon-to-oxygen abundance ratio plotted against the equivalent width of the $3.29\mu\text{m}$ emission band. The error bars on the equivalent widths were obtained from the fits, but no errors are plotted on the C/O ratios as the data were taken from a number of different sources and the uncertainties are generally not listed, but they are expected to be significant. The equivalent width is in nm.

(Roche et al 1996)

Dust Heating

Dust scatters and absorbs short wavelength light, with an efficiency $Q(\nu)$, where Q_{abs} is the ratio of the absorption cross section to the geometric cross section

The optical depth is a function of Q and the column of grains. Dust is heated by absorption of optical/UV photons and radiates in the IR, so that dust particles in equilibrium with the radiation field are governed by:

$$\pi a^2 \int_0^\infty \frac{L_\nu}{4\pi d^2} Q_{abs}(\nu) d\nu = 4\pi a^2 \int_0^\infty Q_{em}(\nu) \pi B_\nu(T_{gr}) d\nu$$

The LHS has the area cross section, the luminosity of the star, diluted by distance d and the absorption coefficient Q_{abs} .

The RHS describes the dust emission from surface area $4\pi a^2$ with an emission coefficient Q_{em} at a temperature T_{gr} .

Note that for IS grains, the albedo (fraction of light reflected) is quite high and that the emissivity in the IR is much lower than in the visible.

For $Q_a/Q_e \sim 10$, $T \sim 500$ K for grains heated by the sun at 1 AU
c.f. ~ 275 K for a blackbody- but reduced by albedo factor.

Emitting grains

Grains do not emit as blackbodies; they are inefficient radiators with low emissivity at long wavelengths.

If grains are small, emission from individual grains will be optically thin, and the emission will be proportional to the volume i.e. $\propto 4/3 \pi a^3 N_{gr} Q_{IR} B(\nu, T)$, whereas the absorption at short wavelengths is proportional to the cross section: $\propto \pi a^2 N_{gr} Q_{abs}$ so that τ_{IR}/τ_{UV} is proportional to the radius, a

As a first step, we can take Planck-averaged efficiencies in the UV and IR $\langle Q_{UV} \rangle$ and $\langle Q_{IR} \rangle$ in which case the expression becomes:

$$\frac{L_*}{4\pi d^2} \langle Q_{UV} \rangle \approx 4 \langle Q_{IR} \rangle \sigma T_{gr}^4$$

The efficiencies are a function of grain composition, temperature and size (small grains radiate less efficiently, and hot grains radiate at shorter wavelengths).

E.g. amorphous carbon has $Q \propto \lambda^{-1}$ and $\langle Q_{IR} \rangle \approx 7 \times 10^{-4} a_{\mu m} T_{gr}$

Emission and Absorption

Because they radiate less efficiently, small grains attain higher temperatures than large grains. We therefore expect a broad range of temperatures from a grain population.

Consider a bimodal small grain population with Larger (ℓ) and Smaller (s) grains with $a_\ell/a_s = 10$ and $(\tau_{UV})_\ell/(\tau_{UV})_s = 10$

Then : $(\tau_{UV})_\ell/(\tau_{IR})_\ell = (\tau_{UV})_s/(\tau_{IR})_s a_\ell/a_s$
and as $\tau_{IR}/\tau_{UV} \propto a$, $(\tau_{IR})_\ell/(\tau_{IR})_s = a^2 = 100$

The small grains may absorb efficiently in the UV, and have bright emission in the IR, but contribute little to absorption in the IR

This is believed to be the explanation for the mid-infrared PAH bands which are prominent in emission but weak in absorption.

Other Heating Mechanisms

In addition to direct heating by starlight, we may need to consider:

Ly alpha heating: trapped line emission from Lyman alpha 1216Å and other resonance lines (e.g. C iv $\lambda 1550$, N v $\lambda 1240$ or Si iv $\lambda 1400$ Å) in HII regions have high optical depths and so a high probability of being absorbed by dust grains.

In ionized regions, this process can maintain grain temperatures above the equilibrium temperature for direct stellar heating, being enhanced in region of high density.

Photoelectric heating of gas by dust is important in the ISM: electrons ejected from grains on absorption of UV photons heat the diffuse gas.

Composition includes at least:
 Silicates, Carbon, PAHs
 (+ ices in cold dense regions)
 Grain size distribution
 $N(a) \approx CN_H a^{-3.5}$ between a_{\min} and a_{\max}
 ($\sim 10 \text{ \AA} < a < 0.25 \mu\text{m}$).

Lower limit is uncertain from
 extinction measurement as when
 $a \ll \lambda/2\pi$ (in the Rayleigh limit), the
 extinction per unit mass is insensitive
 to size but IR emission (PAHs)
 indicates that the particles extend
 down to a few \AA
 A hard upper limit to grain size is not
 very likely (large grains are found in
 meteorites), so may use a roll off of
 the form $N(a) \approx CN_H a^{-3.5} \exp(-a/a_0)$

The grain size distribution in the ISM
 depends on injection, fragmentation
 and growth, with different
 contributions in different regions.

Grain Models

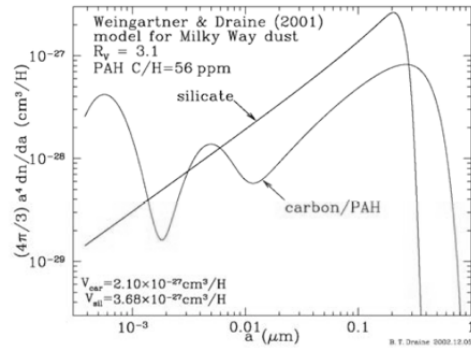


Figure 8: Size distributions for carbonaceous-silicate grain model of Weingartner & Draine (2001)

Dust Mass Estimates

At long wavelengths, dust emission is optically thin,
 so the specific intensity $I_\nu \approx \tau_\nu B(\nu, T)$ and so $S_\nu \approx \int \tau_\nu B(\nu, T) dA / D^2$

$$S_\nu \approx \kappa_\nu B(\nu, T) M_{\text{dust}} / D^2$$

$$M_{\text{dust}} \propto S_\nu D^2 / \kappa_\nu B(\nu, T)$$

Rearranging,

where S_ν is the flux density, κ_ν is the mass absorption coefficient
 [e.g. Hildebrand 1983]

At long wavelengths, we may invoke the Rayleigh Jeans approximation:

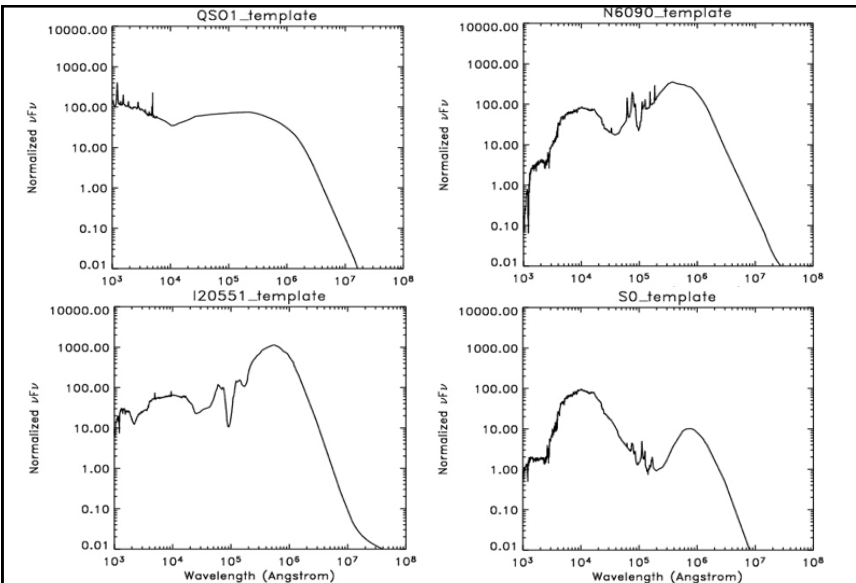
$$B(\nu, T) = 2\pi\nu^2 kT / c^2 \Rightarrow M_{\text{dust}} \propto S_\nu D^2 / T \kappa_\nu$$

Fits typically invoke a spectral index for the opacity, and one or two
 temperature components,

Thermal emission peaks at 50-200 μm

R-J tail relatively insensitive to T_{dust} so gives reasonable estimate of M_{dust} -
 providing opacity known,

could be significant dust mass hidden in cold component
 can have significant optical depths at $\lambda < 60 \mu\text{m}$
 may need to correct for synchrotron or free-free emission



Galaxy SED templates from UV to mm wavelengths, showing variations in dust to optical
 emission, reflecting different dust content and distribution. (M Polletta et al. 2007).

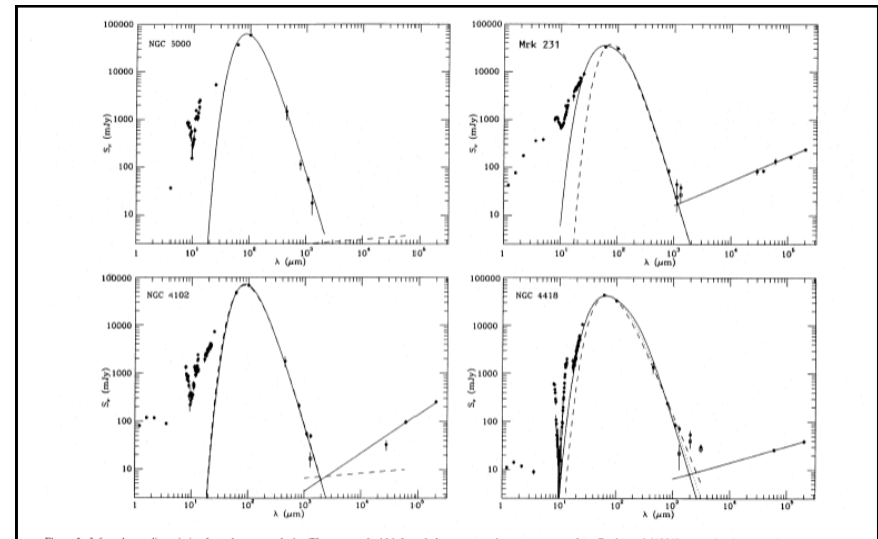


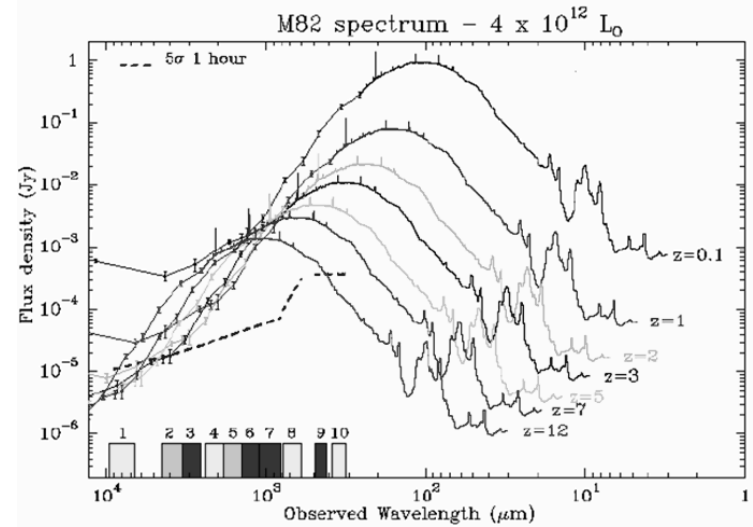
Figure 10: Infrared-to-radio emission from the target galaxies. The near- and mid-infrared photometry and spectroscopy are from Roche et al. (1991), except for the near-infrared photometry of Mrk 231 which is taken from Rieke (1976) and the 4.1- μm datum for NGC 6000 which is the continuum level reported by DePoy (1987). The 12-100 μm photometric points are taken from the IRAS Point Source Catalog, while the 450 μm -2 mm photometry is from the present work. The radio points are taken from Condon et al. (1990), Eales et al. (1990), Gioia et al. (1982) and Kojima et al. (1976). The solid lines through the far-infrared and submillimetre data represent emission from isothermal dust grains, with ν^2 emissivity functions, and source sizes equated to the radio core sizes. These have dust temperatures of 38, 75 and 85 K and diameters of 3, 0.5 and 0.4 arcsec for NGC 4102, NGC 4418 and Mrk 231 respectively. Dashed lines represent emission from optically thin dust with $\beta=2.0$ at temperatures of 34 K in NGC 4102 and NGC 6000 and 38 K in Mrk 231, and with $\beta=1.0$ at 55 K in NGC 4418. The dotted line in NGC 4418 represents emission from a 78-K source of 0.5-arcsec diameter with $\beta=1.5$. The dashed and solid straight lines longwards of 1 mm represent thermal and non-thermal radio components. Open squares indicate the level of excess emission above the dust component for Mrk 231, NGC 4102 and NGC 4418.

Table 2. Spectral indices and mass estimates.

| Object | Distance (Mpc) ^a | Radio Size arcsec ^b | 450/1100 μm spectral index | T_{dust}^c | M_{dust}^d (M_{\odot}) | M_{CO}^e (M_{\odot}) |
|----------|-----------------------------|--------------------------------|---------------------------------------|---------------------|-------------------------------------|-----------------------------------|
| NGC 4102 | 12 | 3.3×2.2 | 3.8 ± 1.1 | 38 | 3.0×10^8 | 1.0×10^9 |
| NGC 4418 | 29 | 0.5×0.3 | 3.1 ± 0.6 | ≈ 75 | $\approx 8 \times 10^8$ | 1.1×10^9 |
| NGC 6000 | 27 | 0.4×0.3 | 3.6 ± 1.7 | 34 | 1.5×10^9 | |
| Mrk 231 | 170 | 0.4×0.3 | | ≈ 85 | $\approx 8 \times 10^9$ | 1.5×10^{10} |

Notes: ^adistances with $H_0 = 75 \text{ km s}^{-1} \text{ Mpc}^{-1}$; ^bradio core sizes measured by Condon et al. (1990) with the VLA; ^cdust temperatures obtained by equating the size of the dust-emitting region to the radio core sizes; ^dtotal mass of molecular material derived from the dust emission, assuming the opacities by Draine & Lee (1984); ^emolecular mass derived from CO measurements by Young & Devereux (1991: NGC 4102) and Sanders et al. (1991: NGC 4418 and Mrk 231), corrected for the distances given in column 2.

(Roche & Chandler 1993)

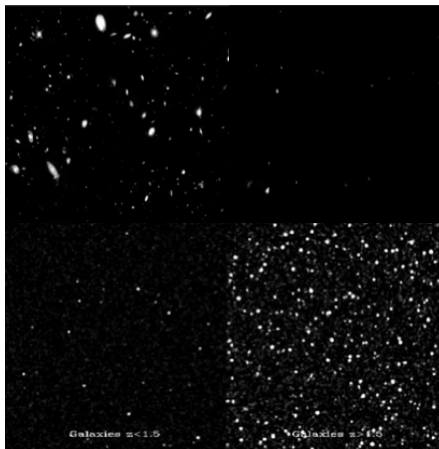


At $\sim 1\text{mm}$ wavelength, star-forming galaxies at redshifts between 0 and 10 may have approximately constant flux as the dust emission peak shifts longwards. This is illustrated here where the spectrum of the nearby starburst galaxy M82 is redshifted out to $z=12$.

Hubble Deep Field: rich in nearby galaxies, poor in distant galaxies.

Nearby galaxies in HDF

Distant galaxies in HDF



Source: K. Lanzetta, SUNY-SB

Source: Wootten and Gallimore, NRAO

Nearby galaxies in ALMA DF

Distant galaxies in ALMA DF

ALMA deep field: poor in nearby galaxies, rich in distant galaxies.

Stochastic emission

Small grains have a small cross section σ_{gr} and so absorb high energy photons only occasionally from the interstellar radiation field.

They have a small thermal capacity, so the temperature increases sharply on photon absorption

This leads to thermal spiking, rather than equilibrium thermal emission

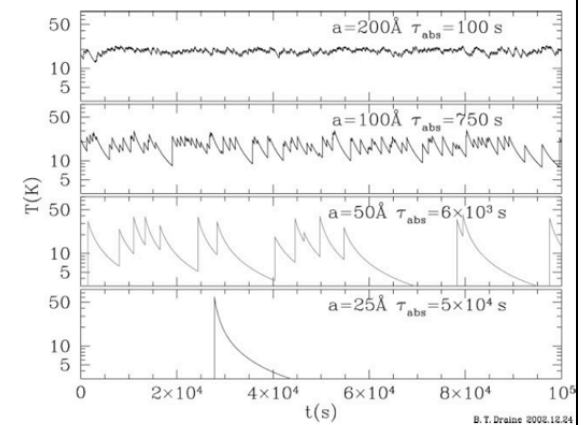


Figure 13 A day in the life of four carbonaceous grains, heated by the local interstellar radiation field. τ_{abs} is the mean time between photon absorptions (Draine & Li 2001).

Thermal spiking

- Grain has heat capacity $C_v \approx 3Nk_B$, where N is the number of atoms in the grain
- The temperature attained $\sim hv/3Nk_B$, so a grain of $\sim 10\text{\AA}$ absorbing a 10eV photon will heat up by $\sim 1000\text{K}$. This energy will be distributed through vibrational modes which will radiate, cooling the grain.
- If high energy photons are absorbed, atoms may be ejected, leading to evaporation and eventually destruction of the grain.
- Note that stochastically heated grains reach temperatures that are independent of distance from the source of photons, though the spiking frequency will be affected.
- This neatly accounts for the similarity of mid-IR spectra from diffuse regions (IR Cirrus) and starburst galaxies
- The boundary between small grains and large molecules is fuzzy.
- Interstellar PAHs are isolated, partially hydrogenated and ionized making laboratory comparisons challenging

Polycyclic Aromatic Hydrocarbons

Detected via a family of narrow emission bands between 3 and $20\mu\text{m}$.

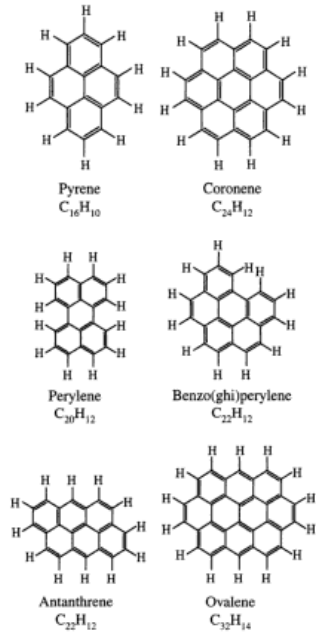
Prominent in neutral zones at the edge of HII regions

Weak or absent within ionized regions and in the circumnuclear regions of AGN – destroyed by high energy photons

Strongly correlated with Carbon abundance in Planetary Nebulae

Band frequencies coincident with C-H and C-C bending and stretching modes in aromatic hydrocarbons

Attributed to compact PAH species



Infrared
Visible

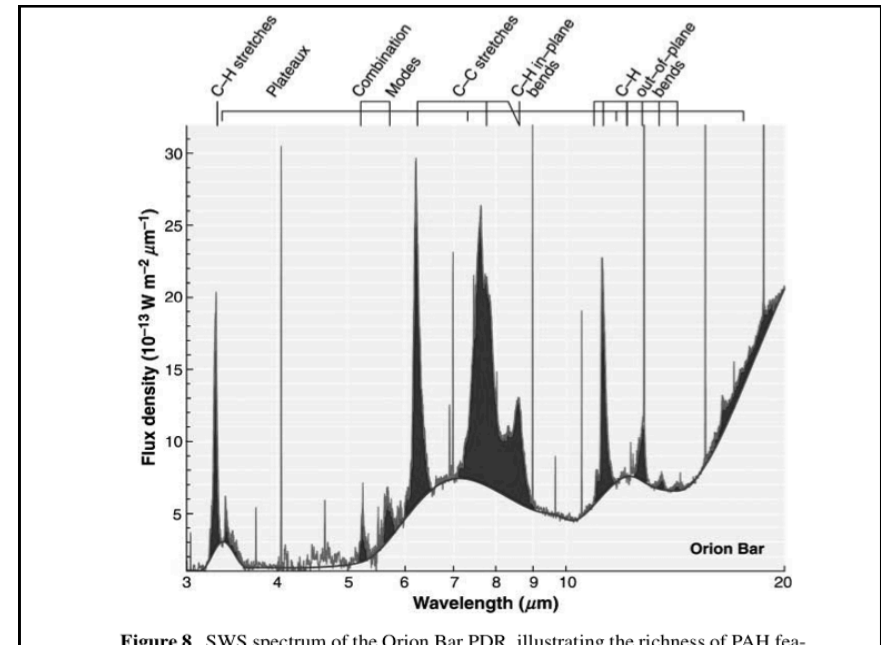
PAHs in the ISM

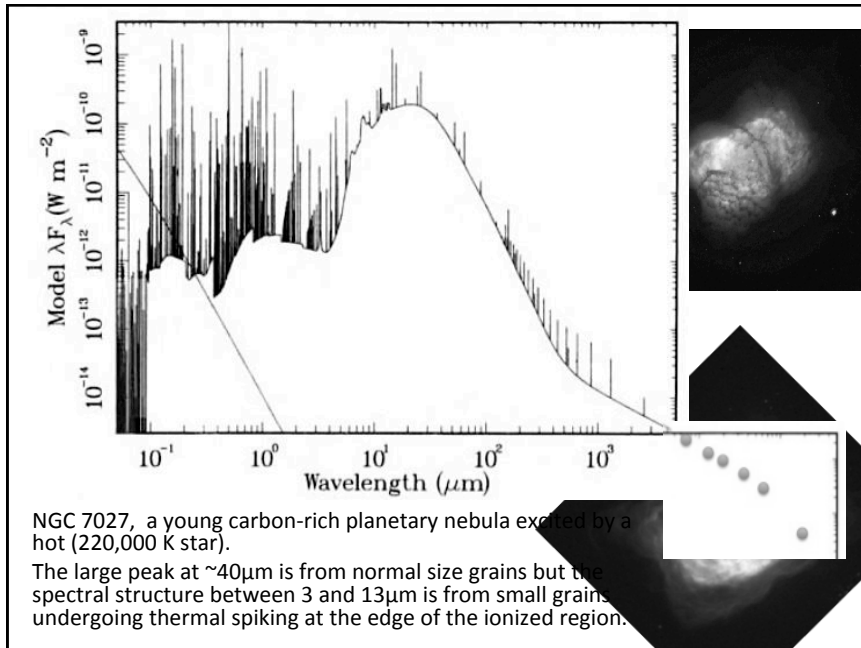
- Mid-Infrared PAH bands trace the interface regions between nebulae and the ISM
- Reveal a new region of excited molecules and low-ionization gas

IR Image (JC000 WFLS200PA)

ISOCAM (8" pixel) Filter LW10

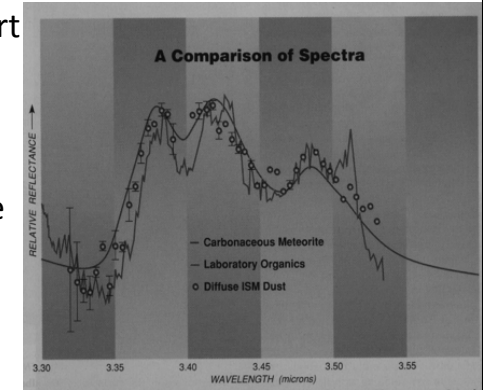
An Orion Nebula Comparison
 Spitzer Space Telescope
 Visible: NGAO/AURA/NSF/A. Blox
 NASA / JPL-Caltech / S.T. Megeath (University of Toledo, Ohio)





Interstellar and Solar System Dust

- Organic materials – hydrocarbons with short chain aliphatic groups (CH_2 , CH_3)
- Found in the diffuse ISM, but polarization measurements indicate a separate component to the silicate grains
- Laboratory Meteorite analysis of Carbonaceous Chondrites



Galactic Recycling

- Stellar outflows $\sim 5 M_{\odot} / \text{yr}$
- But similar amount used up in star formation
- But leads to steady enrichment of heavy elements, nucleosynthesis products over time
- Different dust products from different types of star, and therefore a different mix in different regions
- Condensation of volatile molecules in cold regions
- Dust destruction and fragmentation by supernova shocks, outflows
- Dust growth through coagulation and condensation
- Processing by photons and cosmic rays

